ISSN 2079-1704. Хімія, фізика та технологія поверхні. 2025. Т. 16. № 3. С. 360-375

UDC 544.723:544.18 doi: 10.15407/hftp16.03.360

Fatemeh Mollaamin

MODELING HYDROGEN-CAPTURE WITH SnO_2–SiO_2-BASED MATERIALS DOPED BY ALKALI METAL

Department of Biomedical Engineering, Faculty of Engineering and Architecture, Kastamonu University Kastamonu, Turkey, E-mail: fmollaamin@kastamonu.edu.tr

A vast study on H-capture by LiRb (SnO_2-SiO_2), LiCs(SnO_2-SiO_2), NaRb(SnO_2-SiO_2), NaCs(SnO_2-SiO_2), KRb(SnO_2-SiO_2), KCs(SnO_2-SiO_2), was carried out including using DFT computations at the CAM–B3LYP–D3/6–311+G (d,p) level of theory. The hypothesis of the hydrogen adsorption phenomenon was figured out by density distributions of CDD, TDOS/OPDOS, LOL for nanoclusters of LiRb(SnO_2-SiO_2)–$2H_2$, LiCs(SnO_2-SiO_2)–$2H_2$, NaRb(SnO_2-SiO_2)–$2H_2$, NaCs(SnO_2-SiO_2)–$2H_2$, KRb(SnO_2-SiO_2)–$2H_2$, KCs(SnO_2-SiO_2)–$2H_2$. The oscillation in charge density amounts displays that the electronic densities were mainly placed in the edge of adsorbate/adsorbent atoms during the adsorption status. Regarding optimal energy, KRb(SnO_2-SiO_2), KRb(SnO_2-SiO_2)–$2H_2$, KCs(SnO_2-SiO_2), and KCs(SnO_2-SiO_2)–$2H_2$ heteroclusters have shown more stability than LiRb(SnO_2-SiO_2), LiRb(SnO_2-SiO_2)–$2H_2$, LiCs(SnO_2-SiO_2), LiCs(SnO_2-SiO_2)–$2H_2$, NaRb(SnO_2-SiO_2), NaRb(SnO_2-SiO_2)–$2H_2$, NaCs(SnO_2-SiO_2), NaCs(SnO_2-SiO_2)–$2H_2$ heteroclusters. In this research, hydrogen energy sources on functionalized 2D materials by metals have been shown as promising alternatives for clean energy systems. In a particular way, we have demonstrated here that (SnO_2-SiO_2) weakly adsorbs H_2. At the same time, the Li/Na/K decoration significantly enhances the H_2 interaction, accommodating to H_2 molecules by a stronger physisorption.

Keywords: *Energy storage, alkali metal-ion battery, density of states, charge distribution, materials modeling, hydrogen adsorption*

INTRODUCTION

Sodium/potassium-ion can be the prime chemistry replacement candidate for LIBs [1–6]. The potassium-ion has certain privileges over analogous lithium-ion like the cell design is plain, and both the material and the construction methods are cheaper. The major benefit is the high amount and low cost of potassium in evaluation with lithium, which makes potassium batteries an engaged replacement for large scale batteries like household energy-saving and electric devices. Another privilege of a potassium-ion battery over a lithium-ion battery is potentially charging in a short time [7–13].

Lately, Si-, Ge- or Sn-carbide nanostructures have been proposed as occupied H-grabbing compounds [14–16]. Whereas the polarizability of Si is more than C atom, it is assumed that Si–C/Si nanosheet might append to compositions more strongly in comparison to the pure C-nanostructures [17–19]. The previous investigations of energy-saving devices through H-adsorption have been tailored owing to DFT calculations with a semiconductor group of Si/Ge/Sn/Pb nano-carbides [20], Mg-Al nanoalloy [21] and Al/C/ Si doping of BN nanocomposite [22].

Nanomaterials with notable structures detect undertaking demands in the field of electrocatalysis, fuel cells, and energy-saving. Furthermore, rubidium and cesium ions are studied as electrolyte additives for sodium-ion batteries. It is shown that adding small amount of Rb^+ and Cs^+ into the electrolyte significantly modifies the chemical composition of solid electrolyte interphase on hard carbon surfaces, which results in a significant increase in the ionic conductivity and stability of the solid electrolyte interphase [23].

This investigation wants to delve into the feasibility of LiRb (SnO_2-SiO_2), LiCs(SnO_2-SiO_2), NaRb(SnO_2-SiO_2), NaCs(SnO_2-SiO_2), KRb(SnO_2-SiO_2), KCs(SnO_2-SiO_2) nanoclusters for H-storage. Therefore, it was analyzed the physico-chemical properties of mentioned heteroclusters and hydrogenated nanoclusters of LiRb(SnO_2-SiO_2)–$2H_2$, LiCs(SnO_2-SiO_2)–$2H_2$, NaRb(SnO_2-SiO_2)–$2H_2$, NaCs(SnO_2-SiO_2)–$2H_2$, KRb(SnO_2-SiO_2)–$2H_2$, KCs(SnO_2-SiO_2)–$2H_2$.

MATERIALS AND METHODS

Fig. 1 shows alkali metals-based nanoclusters of LiRb (SnO_2-SiO_2), LiCs(SnO_2-SiO_2), NaRb(SnO_2-SiO_2), NaCs(SnO_2-SiO_2),

$KRb(SnO_2\text{-}SiO_2)$, $KCs(SnO_2\text{-}SiO_2)$ which can enhance the H-storage. In our research, the calculations have been done by CAM–B3LYP–D3 /EPR–3 level of theory. Fig. 1 shows the process of hydrogen adsorption by $LiRb(SnO_2\text{-}SiO_2)$, $LiCs(SnO_2\text{-}SiO_2)$, $NaRb(SnO_2\text{-}SiO_2)$, $NaCs(SnO_2\text{-}SiO_2)$, $KRb(SnO_2\text{-}SiO_2)$, $KCs(SnO_2\text{-}SiO_2)$ nanoclusters and hydrogen-adsorbed nanoclusters of $LiRb(SnO_2\text{-}SiO_2)$–$2H_2$, $LiCs(SnO_2\text{-}SiO_2)$–$2H_2$, $NaRb(SnO_2\text{-}SiO_2)$–$2H_2$, $NaCs(SnO_2\text{-}SiO_2)$–$2H_2$, $KRb(SnO_2\text{-}SiO_2)$–$2H_2$, $KCs(SnO_2\text{-}SiO_2)$–$2H_2$.

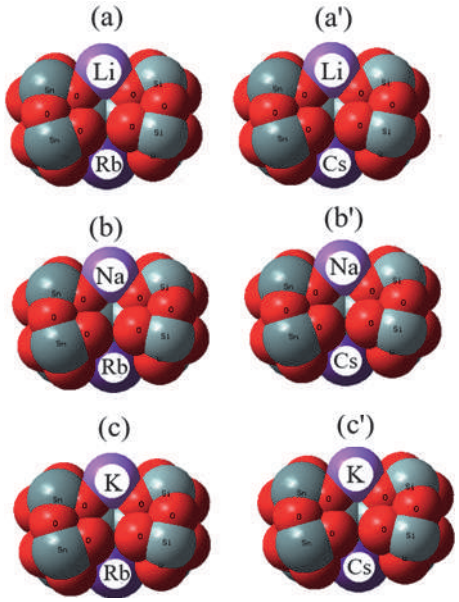

Fig. 1. Adding Li, Na, K to $(SnO_2\text{-}SiO_2)$ nanoclusters accompanying Rb or Cs doping and formation of $LiRb(SnO_2\text{-}SiO_2)$, $LiCs(SnO_2\text{-}SiO_2)$, $NaRb(SnO_2\text{-}SiO_2)$, $NaCs(SnO_2\text{-}SiO_2)$, $KRb(SnO_2\text{-}SiO_2)$, $KCs(SnO_2\text{-}SiO_2)$ nanoclusters towards energy storage through hydrogen adsorption as $LiRb(SnO_2\text{-}SiO_2)$–$2H_2$, $LiCs(SnO_2\text{-}SiO_2)$–$2H_2$, $NaRb(SnO_2\text{-}SiO_2)$–$2H_2$, $NaCs(SnO_2\text{-}SiO_2)$–$2H_2$, $KRb(SnO_2\text{-}SiO_2)$–$2H_2$, $KCs(SnO_2\text{-}SiO_2)$–$2H_2$ in novel batteries

The Bader charge analysis [24] was illustrated during H-atoms grabbing by $LiRb(SnO_2\text{-}SiO_2)$–$2H_2$, $LiCs(SnO_2\text{-}SiO_2)$–$2H_2$, $NaRb(SnO_2\text{-}SiO_2)$–$2H_2$, $NaCs(SnO_2\text{-}SiO_2)$–$2H_2$, $KRb(SnO_2\text{-}SiO_2)$–$2H_2$, $KCs(SnO_2\text{-}SiO_2)$–$2H_2$ nanoclusters (Fig. 1). The rigid potential energy surface using density functional theory [25–27] was performed due to Gaussian 16 revision C.01 program package [28] and GaussView 6.1 [29]. The coordination input for hydrogen grabbing by $LiRb(SnO_2\text{-}SiO_2)$, $LiCs(SnO_2\text{-}SiO_2)$, $NaRb(SnO_2\text{-}SiO_2)$, $NaCs(SnO_2\text{-}SiO_2)$, $KRb(SnO_2\text{-}SiO_2)$, $KCs(SnO_2\text{-}SiO_2)$ has been optimized with LANL2DZ and 6-311+G (d,p) basis sets.

RESULTS AND DISCUSSION

CDD analysis. The charge density differences (CDD) [30] has been shown for $LiRb(SnO_2\text{-}SiO_2)$, $LiCs(SnO_2\text{-}SiO_2)$, $NaRb(SnO_2\text{-}SiO_2)$, $NaCs(SnO_2\text{-}SiO_2)$, $KRb(SnO_2\text{-}SiO_2)$, $KCs(SnO_2\text{-}SiO_2)$ nanoclusters with the fluctuation in the region around –12 to +6 Bohr (Fig. 2 *a–f*) and for the nanoclusters of $LiRb(SnO_2\text{-}SiO_2)$–$2H_2$, $LiCs(SnO_2\text{-}SiO_2)$–$2H_2$, $NaRb(SnO_2\text{-}SiO_2)$–$2H_2$, $NaCs(SnO_2\text{-}SiO_2)$–$2H_2$, $KRb(SnO_2\text{-}SiO_2)$–$2H_2$, $KCs(SnO_2\text{-}SiO_2)$–$2H_2$ (Fig. 2 *a′–f′*) in the area around –12 to +6 Bohr. Furthermore, the atoms of O2, O3, O7–O12, O14, O15, O17, O18, O22–O27, O29, O30 from alkali metal hybrid (Li,Na,K,Rb,Cs)–$(SnO_2\text{-}SiO_2)$ oxide (Fig.2–f) have shown the fluctuation around –12 to +6 Bohr towards formation of hydrogenated alkali metal hybrid (Li,Na,K,Rb,Cs)–$(SnO_2\text{-}SiO_2)$–$2H_2$ through hydrogen adsorption (Fig. 2 *a′–f′*).

The charge distribution has been illustrated during H-capture by $LiRb(SnO_2\text{-}SiO_2)$, $LiCs(SnO_2\text{-}SiO_2)$, $NaRb(SnO_2\text{-}SiO_2)$, $NaCs(SnO_2\text{-}SiO_2)$, $KRb(SnO_2\text{-}SiO_2)$, $KCs(SnO_2\text{-}SiO_2)$ nanoclusters towards formation of $LiRb(SnO_2\text{-}SiO_2)$–$2H_2$, $LiCs(SnO_2\text{-}SiO_2)$–$2H_2$, $NaRb(SnO_2\text{-}SiO_2)$–$2H_2$, $NaCs(SnO_2\text{-}SiO_2)$–$2H_2$, $KRb(SnO_2\text{-}SiO_2)$–$2H_2$, $KCs(SnO_2\text{-}SiO_2)$–$2H_2$, respectively (Tables 1, 2, 3).

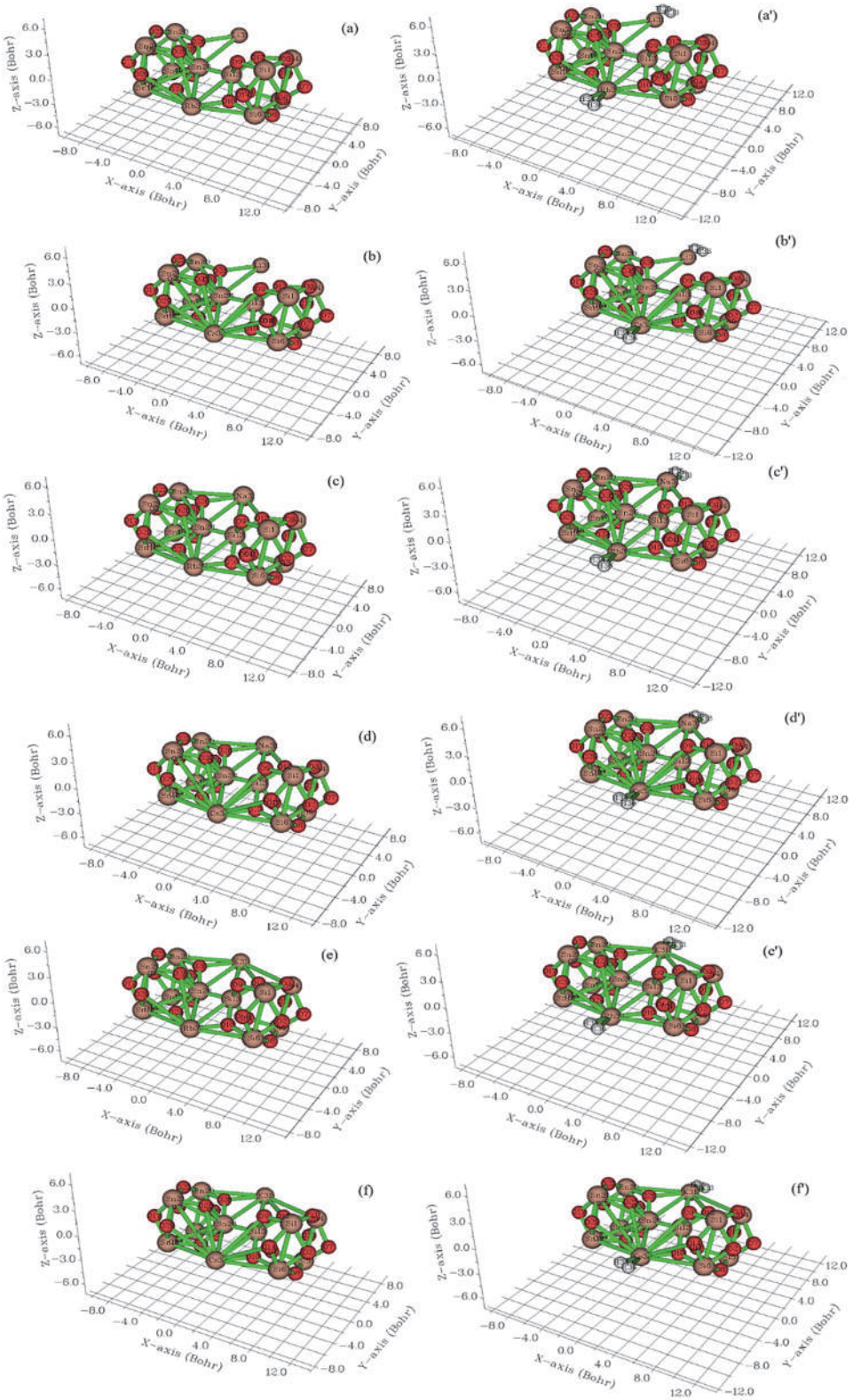

Fig. 2. CDD graphs for (*a*) LiRb (SnO_2-SiO_2), (*a′*) LiRb(SnO_2-SiO_2)–$2H_2$, (*b*) LiCs(SnO_2-SiO_2), (*b′*) LiCs(SnO_2-SiO_2)–$2H_2$, (*c*) NaRb(SnO_2-SiO_2), (*c′*) NaRb(SnO_2-SiO_2)–$2H_2$, (*d*) NaCs(SnO_2-SiO_2), (*d′*) NaRb(SnO_2-SiO_2)–2H2, (*e*) KRb(SnO_2-SiO_2), (*e′*) KRb(SnO_2-SiO_2)–$2H_2$, (*f*) KCs(SnO_2-SiO_2), (*f′*) KCs(SnO_2-SiO_2)–$2H_2$ nanoclusters

Table 1. The atomic charge (*Q*/coulomb) for LiRb(SnO_2-SiO_2), LiRb(SnO_2-SiO_2)–$2H_2$, LiCs(SnO_2-SiO_2), LiCs(SnO_2-SiO_2)–$2H_2$ nanoclusters

LiRb(SnO_2-SiO_2)		**LiRb(SnO_2-SiO_2)–$2H_2$**		**LiCs(SnO_2-SiO_2)**		**LiCs(SnO_2-SiO_2)–$2H_2$**	
Atom	***Q***	**Atom**	***Q***	**Atom**	***Q***	**Atom**	***Q***
Si1	1.4595	Si1	1.4585	Si1	1.4500	Si1	1.4517
O2	-0.6386	O2	-0.7115	O2	-0.6584	O2	-0.6581
O3	-0.8300	O3	-0.8284	O3	-0.8259	O3	-0.8258
Si4	1.4154	Si4	1.4205	Si4	1.4232	Si4	1.4262
Si5	1.4335	Si5	1.4445	Si5	1.4359	Si5	1.4365
Si6	1.4423	Si6	1.4323	Si6	1.3760	Si6	1.3738
O7	-0.7238	O7	-0.6720	O7	-0.7290	O7	-0.7299
O8	-0.8276	O8	-0.8168	O8	-0.8277	O8	-0.8272
O9	-0.8024	O9	-0.7917	O9	-0.8166	O9	-0.8162
O10	-0.9816	O10	-1.0029	O10	-0.9086	O10	-0.9081
O11	-0.8096	O11	-0.8124	O11	-0.8274	O11	-0.8258
O12	-0.9562	O12	-0.9281	O12	-0.9538	O12	-0.9530
Si13	1.3446	Si13	1.3479	Si13	1.3162	Si13	1.3212
O14	-0.7850	O14	-0.7303	O14	-0.8261	O14	-0.8281
O15	-0.7116	O15	-0.7695	O15	-0.7367	O15	-0.7341
Sn16	1.6861	Sn16	1.6845	Sn16	1.6165	Sn 16	1.6118
O17	-0.8023	O17	-0.8002	O17	-0.8033	O17	-0.8024
O18	-0.8753	O18	-0.8740	O18	-0.8735	O18	-0.8723
Sn19	1.6926	Sn19	1.6896	Sn19	1.6857	Sn19	1.6838
Sn20	1.6748	Sn20	1.6738	Sn20	1.6772	Sn20	1.6780
Sn21	1.7000	Sn21	1.6944	Sn21	1.6887	Sn21	1.6847
O22	-0.8478	O22	-0.8487	O22	-0.8428	O22	-0.843
O23	-0.8918	O23	-0.8915	O23	-0.8896	O23	-0.8891
O24	-1.0604	O24	-1.0600	O24	-0.9866	O24	-0.9755
O25	-0.9118	O25	-0.9130	O25	-0.9212	O25	-0.9208
O26	-1.0012	O26	-0.9994	O26	-0.9995	O26	-0.9967
O27	-0.9211	O27	-0.9215	O27	-0.9296	O27	-0.9301
Sn28	1.7090	Sn28	1.7177	Sn28	1.6408	Sn28	1.6453
O29	-0.9053	O29	-0.9077	O29	-0.9280	O29	-0.9300
O30	-0.8585	O30	-0.8575	O30	-0.8664	O30	-0.8675
Li31	0.7100	Li31	0.6000	Li31	0.7114	Li31	0.6084
Rb32	0.8742	Rb32	0.8555	Cs32	1.1292	Cs32	1.1041
		H33	-0.0198			H33	-0.0201
		H34	-0.0121			H34	-0.0106
		H35	0.1210			H35	0.1212
		H36	0.0280			H36	0.0181

Table 2. The atomic charge (Q/coulomb) for $NaRb(SnO_2\text{-}SiO_2)$, $NaRb(SnO_2\text{-}SiO_2)–2H_2$, $NaCs(SnO_2\text{-}SiO_2)$, $NaCs(SnO_2\text{-}SiO_2)–2H_2$ nanoclusters

$NaRb(SnO_2\text{-}SiO_2)$		$NaRb(SnO_2\text{-}SiO_2)–2H_2$		$NaCs(SnO_2\text{-}SiO_2)$		$NaCs(SnO_2\text{-}SiO_2)–2H_2$	
Atom	***Q***	**Atom**	***Q***	**Atom**	***Q***	**Atom**	***Q***
Si1	1.4596	Si1	1.4594	Si1	1.4540	Si1	1.4554
O2	-0.6385	O2	-0.6386	O2	-0.7168	O2	-0.7167
O3	-0.8297	O3	-0.8298	O3	-0.8224	O3	-0.8226
Si4	1.4079	Si4	1.4111	Si4	1.4092	Si4	1.4130
Si5	1.4370	Si5	1.4375	Si5	1.4407	Si5	1.4417
Si6	1.4410	Si6	1.4400	Si6	1.3713	Si6	1.3683
O7	-0.7239	O7	-0.7244	O7	-0.6878	O7	-0.6876
O8	-0.8279	O8	-0.8278	O8	-0.8204	O8	-0.8197
O9	-0.8019	O9	-0.8017	O9	-0.8132	O9	-0.8129
O10	-0.9804	O10	-0.9811	O10	-0.9156	O10	-0.9147
O11	-0.8123	O11	-0.8117	O11	-0.8367	O11	-0.8353
O12	-0.9745	O12	-0.9737	O12	-0.9486	O12	-0.9474
Si13	1.3346	Si13	1.3370	Si13	1.3092	Si13	1.3140
O14	-0.7851	O14	-0.7871	O14	-0.7889	O14	-0.7888
O15	-0.7164	O15	-0.7158	O15	-0.7886	O15	-0.7886
Sn16	1.6926	Sn 16	1.6898	Sn 16	1.6227	Sn 16	1.6182
O17	-0.8030	O17	-0.8020	O17	-0.8037	O17	-0.8028
O18	-0.8769	O18	-0.8760	O18	-0.8760	O18	-0.8746
Sn19	1.6937	Sn19	1.6923	Sn19	1.6883	Sn19	1.6871
Sn20	1.6695	Sn20	1.6721	Sn20	1.6737	Sn20	1.6768
Sn21	1.6995	Sn21	1.6947	Sn21	1.6898	Sn21	1.6864
O22	-0.8483	O22	-0.8481	O22	-0.8433	O22	-0.8433
O23	-0.8906	O23	-0.8900	O23	-0.8882	O23	-0.8877
O24	-1.0573	O24	-1.0562	O24	-0.9832	O24	-0.9737
O25	-0.9110	O25	-0.9105	O25	-0.9206	O25	-0.9201
O26	-1.0314	O26	-1.0292	O26	-1.0304	O26	-1.0283
O27	-0.9219	O27	-0.9222	O27	-0.9295	O27	-0.9301
Sn28	1.7062	Sn28	1.7161	Sn28	1.6445	Sn28	1.6543
O29	-0.9052	O29	-0.9076	O29	-0.9288	O29	-0.9306
O30	-0.8622	O30	-0.8630	O30	-0.8693	O30	-0.8699
Na31	0.7874	Na31	0.7080	Na31	0.7726	Na31	0.6938
Rb32	0.8694	Rb32	0.8503	Cs32	1.1361	Cs32	1.1098
		H33	-0.0260			H33	-0.0233
		H34	-0.0138			H34	-0.0120
		H35	0.0972			H35	0.0948
		H36	0.0308			H36	0.0174

Table 3. The atomic charge (Q/coulomb) for KRb(SnO_2-SiO_2), KRb(SnO_2-SiO_2)–$2H_2$, KCs(SnO_2-SiO_2), KCs(SnO_2-SiO_2)–$2H_2$ nanoclusters

KRb(SnO_2-SiO_2)		**KRb(SnO_2-SiO_2)–$2H_2$**		**KCs(SnO_2-SiO_2)**		**KCs(SnO_2-SiO_2)–$2H_2$**	
Atom	***Q***	**Atom**	***Q***	**Atom**	***Q***	**Atom**	***Q***
Si1	1.4589	Si1	1.4597	Si1	1.4490	Si1	1.4515
O2	-0.63826	O2	-0.6382	O2	-0.6585	O2	-0.6579
O3	-0.8300	O3	-0.8288	O3	-0.8244	O3	-0.8244
Si4	1.4071	Si4	1.4088	Si4	1.4151	Si4	1.4171
Si5	1.4370	Si5	1.4374	Si5	1.4393	Si5	1.4399
Si6	1.4411	Si6	1.4405	Si6	1.3742	Si6	1.3723
O7	-0.7245	O7	-0.7250	O7	-0.7304	O7	-0.7309
O8	-0.8277	O8	-0.8276	O8	-0.8278	O8	-0.8272
O9	-0.7991	O9	-0.7988	O9	-0.8136	O9	-0.8132
O10	-0.9813	O10	-0.9816	O10	-0.9081	O10	-0.9073
O11	-0.8116	O11	-0.8111	O11	-0.8285	O11	-0.8269
O12	-0.9921	O12	-0.9921	O12	-0.9911	O12	-0.9913
Si13	1.3220	Si13	1.3226	Si13	1.2947	Si13	1.2983
O14	-0.7850	O14	-0.7870	O14	-0.8265	O14	-0.8284
O15	-0.7192	O15	-0.7193	O15	-0.7446	O15	-0.7432
Sn16	1.6917	Sn 16	1.6903	Sn16	1.6218	Sn16	1.6185
O17	-0.8033	O17	-0.8024	O17	-0.8041	O17	-0.8032
O18	-0.8766	O18	-0.8757	O18	-0.8747	O18	-0.8735
Sn19	1.6962	Sn19	1.6957	Sn19	1.6895	Sn19	1.6891
Sn20	1.6643	Sn20	1.6667	Sn20	1.6672	Sn20	1.6700
Sn21	1.6984	Sn21	1.6944	Sn21	1.6882	Sn21	1.6855
O22	-0.8471	O22	-0.8463	O22	-0.8422	O22	-0.8415
O23	-0.8873	O23	-0.8867	O23	-0.8852	O23	-0.8847
O24	-1.0583	O24	-1.0570	O24	-0.9853	O24	-0.9745
O25	-0.9086	O25	-0.9084	O25	-0.9179	O25	-0.9177
O26	-1.0605	O26	-1.0607	O26	-1.0588	O26	-1.0600
O27	-0.9193	O27	-0.9197	O27	-0.9278	O27	-0.9284
Sn28	1.6576	Sn28	1.6614	Sn28	1.5917	Sn28	1.5947
O29	-0.9055	O29	-0.9079	O29	-0.9281	O29	-0.9301
O30	-0.8661	O30	-0.8672	O30	-0.8733	O30	-0.8743
K31	0.8941	K31	0.8616	K31	0.8915	K31	0.8597
Rb32	0.8723	Rb32	0.8561	Cs32	1.1289	Cs32	1.1042
		H33	-0.0571			H33	-0.0565
		H34	-0.0139			H34	-0.0110
		H35	0.0864			H35	0.0860
		H36	0.0309			H36	0.0183

The atomic charge of Si, Sn,O and alkali metals of Li, Na, K,Rb,Cs and hydrogen atoms absorbed on LiRb (SnO_2-SiO_2), LiCs(SnO_2-SiO_2), NaRb(SnO_2-SiO_2), NaCs(SnO_2-SiO_2), KRb(SnO_2-SiO_2), KCs(SnO_2-SiO_2) nanoclusters have been evaluated. Functionalizing lithium, sodium and potassium atoms can augment the negative atomic charge of O2, O3, O7–O12, O14, O15, O17, O18, O22–O27, O29, O30 in LiRb (SnO_2-SiO_2), LiCs(SnO_2-SiO_2), NaRb(SnO_2-SiO_2), NaCs(SnO_2-SiO_2), KRb(SnO_2-SiO_2), KCs(SnO_2-SiO_2) nanoclusters. In fact, LiRb (SnO_2-SiO_2), LiCs(SnO_2-SiO_2), NaRb(SnO_2-SiO_2), NaCs(SnO_2-SiO_2), KRb(SnO_2-SiO_2), KCs(SnO_2-SiO_2) nanoclusters have shown more efficiency than (SnO_2-SiO_2) cluster [30] for electron acceptance from electron donor of H33, H34, H35 and H36 (Tables 1, 2, 3).

The changes of charge density analysis in the adsorption process have illustrated that LiRb (SnO_2-SiO_2) and LiCs(SnO_2-SiO_2) has shown the Bader charge of –1.709 and –1.689 coulomb before hydrogen adsorption and –1.718 and –1.685 coulomb after hydrogen adsorption. Moreover, the changes of charge density analysis for NaRb(SnO_2-SiO_2), NaCs(SnO_2-SiO_2) has shown the Bader charge of –1.706 and –1.690 coulomb before hydrogen adsorption and –1.716 and –1.687 coulomb after hydrogen adsorption. KRb(SnO_2-SiO_2) and KCs(SnO_2-SiO_2) have shown the Bader charge of –1.698 and –1.689 coulomb before hydrogen adsorption and –1.696 and –1.689 coulomb after hydrogen adsorption.

The differences of charge density for these structures are measured as: $\Delta Q_{LiRb(SnO2\text{-}SiO2)} = -0.009$, $\Delta Q_{LiCs(SnO2\text{-}SiO2)} = 0.004$, $\Delta Q_{NaRb(SnO2\text{-}SiO2)} = -0.01$, $\Delta Q_{NaCs(SnO2\text{-}SiO2)} = 0.003$, $\Delta Q_{KRb(SnO2\text{-}SiO2)} = 0.002$, $\Delta Q_{KCs(SnO2\text{-}SiO2)} = 0$ coulomb. Therefore, the results have shown that the cluster of NaRb(SnO_2-SiO_2), LiRb(SnO_2-SiO_2), KRb(SnO_2-SiO_2), and may have the most tensity for electron accepting owing to hydrogen capture.

TDOS/OPDOS analysis. The energy levels in an isolated system (such as molecule), are discrete, the concept of density of state (DOS) is supposed to be completely valueless in this situation. Therefore, the original total DOS (TDOS) of isolated system can be written as [31]:

$$TDOS\ (E) = \sum_i \delta\ (E - \epsilon_i\ )\ . \qquad (1)$$

The normalized Gaussian function is defined as:

$$G(x) = \frac{1}{c\sqrt{2\pi}} e^{-\frac{x^2}{2c^2}} \text{ where } c = \frac{\text{FWHM}}{2\sqrt{2\ln x}}. \qquad (2)$$

FWHM (full width at half maximum) is an adjustable parameter in Multiwfn. In the TDOS map, each discrete vertical line corresponds to a molecular orbital (MO), the dashed line highlights the position of HOMO. The curve is the TDOS simulated based on the distribution of MO energy levels.

Regarding adsorption behavior of hydrogen by LiRb (SnO_2-SiO_2), LiCs(SnO_2-SiO_2), NaRb(SnO_2-SiO_2), NaCs(SnO_2-SiO_2), KRb(SnO_2-SiO_2), KCs(SnO_2-SiO_2) nanoclusters, TDOS has been measured. This parameter can indicate the existence of important chemical interactions often on the convex side (Fig. 3 *a–f*, *a′–f′*).

During formation of LiRb (SnO_2-SiO_2), LiCs(SnO_2-SiO_2), NaRb(SnO_2-SiO_2), NaCs(SnO_2-SiO_2), KRb(SnO_2-SiO_2) (Fig. 3 *a*, *b*, *c*, *d*, *e*) and hydrogenated nanoclusters containing LiRb(SnO_2-SiO_2)–$2H_2$, LiCs(SnO_2-SiO_2)–$2H_2$, NaRb(SnO_2-SiO_2)–$2H_2$, NaCs(SnO_2-SiO_2)–$2H_2$ (Fig. 3 *a′*, *b′*, *c′*, *d′*, *e′*) have shown the steepest peaks around –0.3, –0.45 and –0.60 a.u. due to covalent bond between two atoms of Li/Rb, Li/Cs, Na/Rb, Na/Cs with (SnO_2-SiO_2) nanocluster.

However, the TDOS curve for KRb (SnO_2-SiO_2) and KRb (SnO_2-SiO_2)–$2H_2$ nanoclusters have shown four pointed peaks around –0.3, –0.45, –0.60, –0.75 a.u. due to covalent bond between atoms of K, Rb, Cs with (SnO_2-SiO_2) nanocluster through hydrogen storage with maximum density of state of ≈ 24 around –0.30 a.u. (Fig. 3 *f*, *f′*).

Fragment 1 has been defined for O9 to O12, Si13, O24 to O27 and Sn28, X31(X = Li, Na,K)/Y32 (Y = Rb, Cs) in Fig. 3 *a–f* and H36 to H36 in Fig. 3 *a′–f′*. Fragment 2 has indicated the fluctuation of Si1, Si4 to Si6 beside the similar involved atoms of Fragment 1 in Fig. 3 *a*, *b*, *c*, *d* and Fig. 3 *a′–f′*. Finally, it was considered the fluctuation of Sn16, Sn19 to Sn21, O17, O18, O22, O23, O29, O30 in Fig. 3 *a–f*, *a′–f′* through Fragment 3.

LOL analysis. Localized orbital locator (LOL) has a similar expression compared to electron localization function (ELF) [32].

$$\text{LOL}(\mathbf{r}) = \frac{\tau(\mathbf{r})}{1+\tau(\mathbf{r})}; \tau(\mathbf{r}) = \frac{D_0(\mathbf{r})}{\frac{1}{2}\sum_i \eta_i |\nabla \varphi_i\ (\mathbf{r})|^2}, \qquad (3)$$

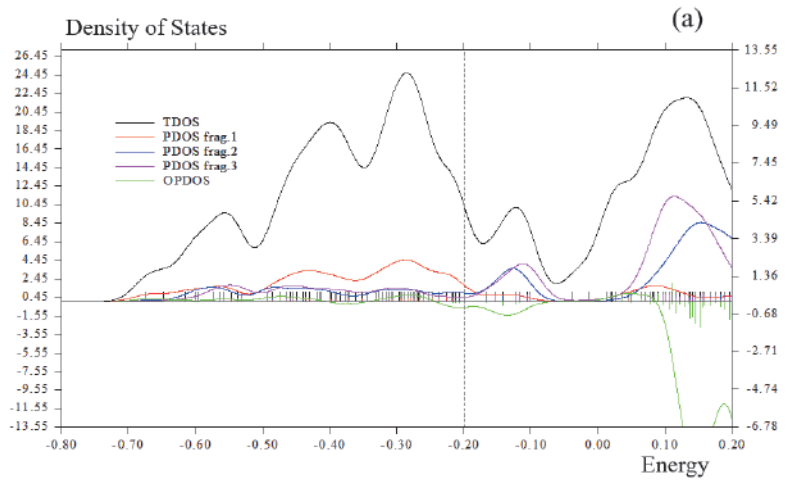
Density of States
(a)
TDOS
PDOS frag.1
PDOS frag.2
PDOS frag.3
OPDOS
26.45 24.45 22.45 20.45 18.45 16.45 14.45 12.45 10.45 8.45 6.45 4.45 2.45 0.45 -1.55 -3.55 -5.55 -7.55 -9.55 -11.55 -13.55
13.55 11.52 9.49 7.45 5.42 3.39 1.36 -0.68 -2.71 -4.74 -6.78
-0.80 -0.70 -0.60 -0.50 -0.40 -0.30 -0.20 -0.10 0.00 0.10 0.20
Energy

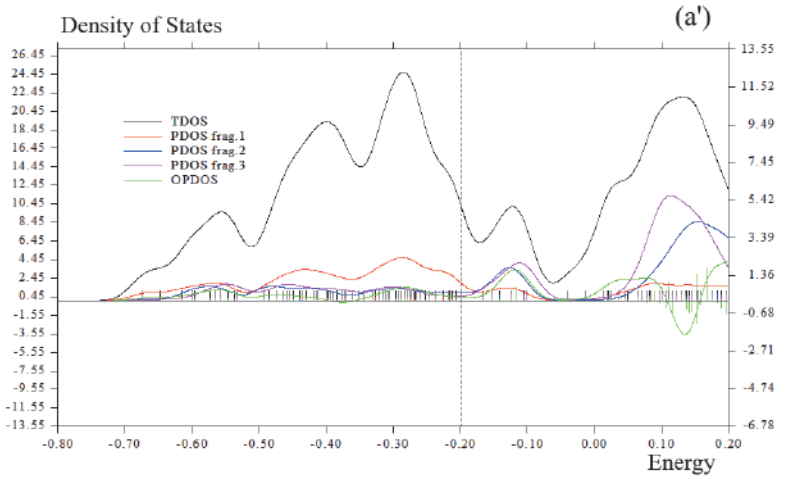
Density of States
(a')
TDOS
PDOS frag.1
PDOS frag.2
PDOS frag.3
OPDOS
26.45 24.45 22.45 20.45 18.45 16.45 14.45 12.45 10.45 8.45 6.45 4.45 2.45 0.45 -1.55 -3.55 -5.55 -7.55 -9.55 -11.55 -13.55
13.55 11.52 9.49 7.45 5.42 3.39 1.36 -0.68 -2.71 -4.74 -6.78
-0.80 -0.70 -0.60 -0.50 -0.40 -0.30 -0.20 -0.10 0.00 0.10 0.20
Energy

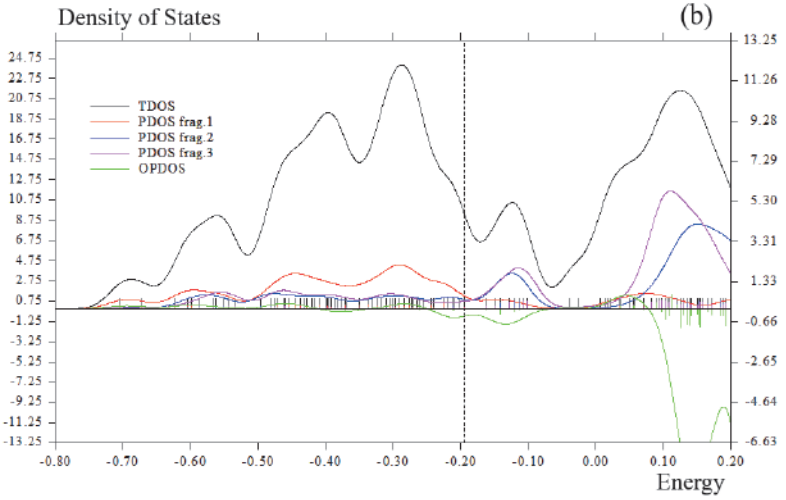
Density of States
(b)
TDOS
PDOS frag.1
PDOS frag.2
PDOS frag.3
OPDOS
24.75 22.75 20.75 18.75 16.75 14.75 12.75 10.75 8.75 6.75 4.75 2.75 0.75 -1.25 -3.25 -5.25 -7.25 -9.25 -11.25 -13.25
13.25 11.26 9.28 7.29 5.30 3.31 1.33 -0.66 -2.65 -4.64 -6.63
-0.80 -0.70 -0.60 -0.50 -0.40 -0.30 -0.20 -0.10 0.00 0.10 0.20
Energy

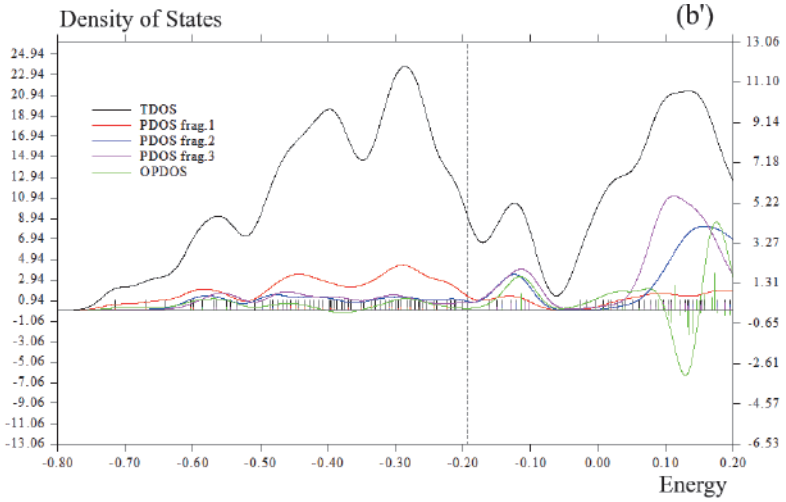
Density of States
(b')
TDOS
PDOS frag.1
PDOS frag.2
PDOS frag.3
OPDOS
24.94 22.94 20.94 18.94 16.94 14.94 12.94 10.94 8.94 6.94 4.94 2.94 0.94 -1.06 -3.06 -5.06 -7.06 -9.06 -11.06 -13.06
13.06 11.10 9.14 7.18 5.22 3.27 1.31 -0.65 -2.61 -4.57 -6.53
-0.80 -0.70 -0.60 -0.50 -0.40 -0.30 -0.20 -0.10 0.00 0.10 0.20
Energy

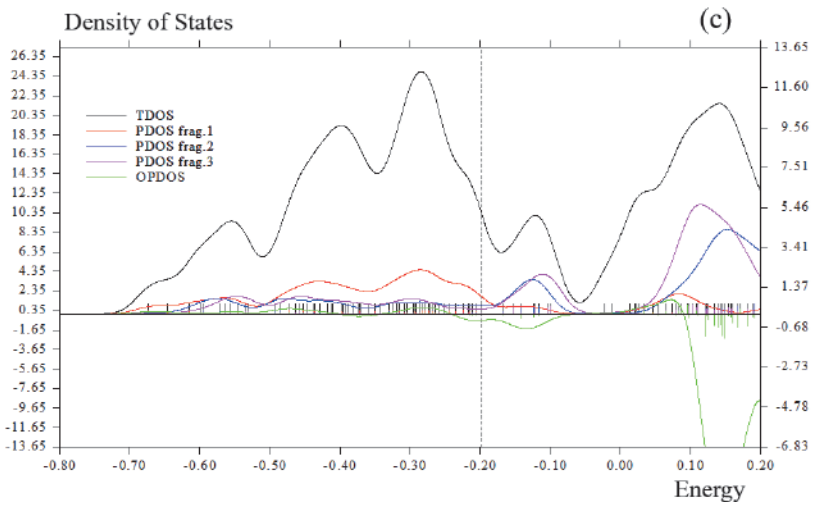
Density of States
(c)
TDOS
PDOS frag.1
PDOS frag.2
PDOS frag.3
OPDOS
26.35 24.35 22.35 20.35 18.35 16.35 14.35 12.35 10.35 8.35 6.35 4.35 2.35 0.35 -1.65 -3.65 -5.65 -7.65 -9.65 -11.65 -13.65
13.65 11.60 9.56 7.51 5.46 3.41 1.37 -0.68 -2.73 -4.78 -6.83
-0.80 -0.70 -0.60 -0.50 -0.40 -0.30 -0.20 -0.10 0.00 0.10 0.20
Energy

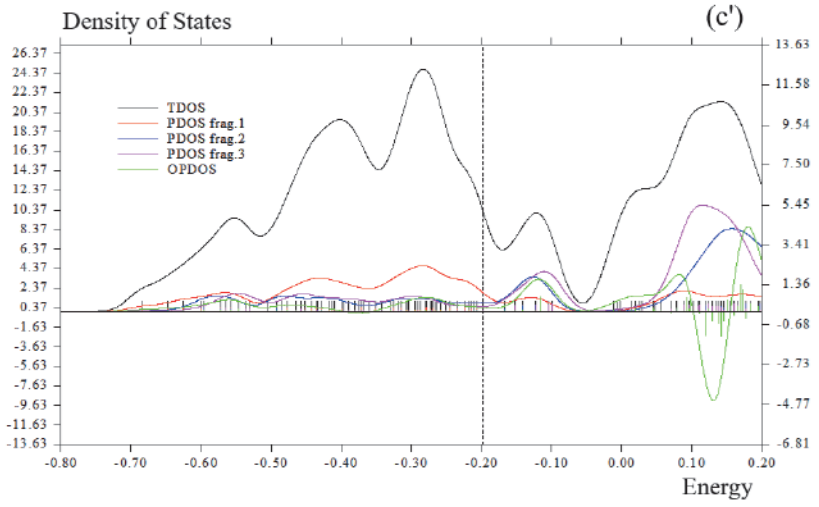
Density of States
(c')
TDOS
PDOS frag.1
PDOS frag.2
PDOS frag.3
OPDOS
26.37 24.37 22.37 20.37 18.37 16.37 14.37 12.37 10.37 8.37 6.37 4.37 2.37 0.37 -1.63 -3.63 -5.63 -7.63 -9.63 -11.63 -13.63
13.63 11.58 9.54 7.50 5.45 3.41 1.36 -0.68 -2.73 -4.77 -6.81
-0.80 -0.70 -0.60 -0.50 -0.40 -0.30 -0.20 -0.10 0.00 0.10 0.20
Energy

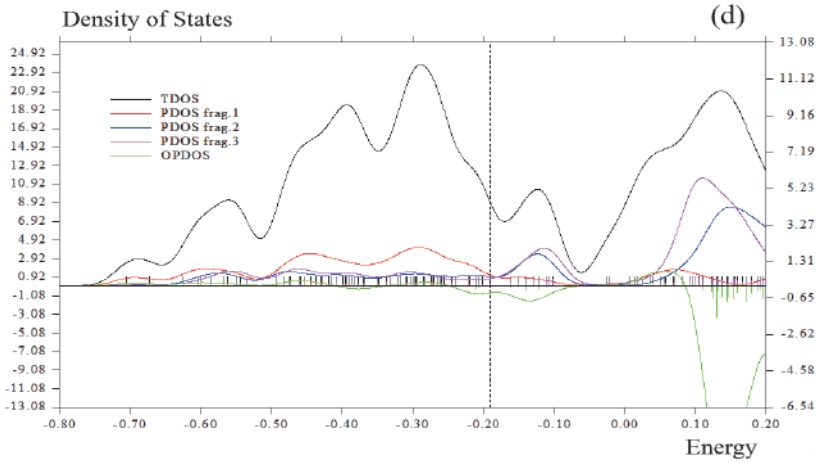
Density of States
(d)
TDOS
PDOS frag.1
PDOS frag.2
PDOS frag.3
OPDOS
24.92 22.92 20.92 18.92 16.92 14.92 12.92 10.92 8.92 6.92 4.92 2.92 0.92 -1.08 -3.08 -5.08 -7.08 -9.08 -11.08 -13.08
13.08 11.12 9.16 7.19 5.23 3.27 1.31 -0.65 -2.62 -4.58 -6.54
-0.80 -0.70 -0.60 -0.50 -0.40 -0.30 -0.20 -0.10 0.00 0.10 0.20
Energy

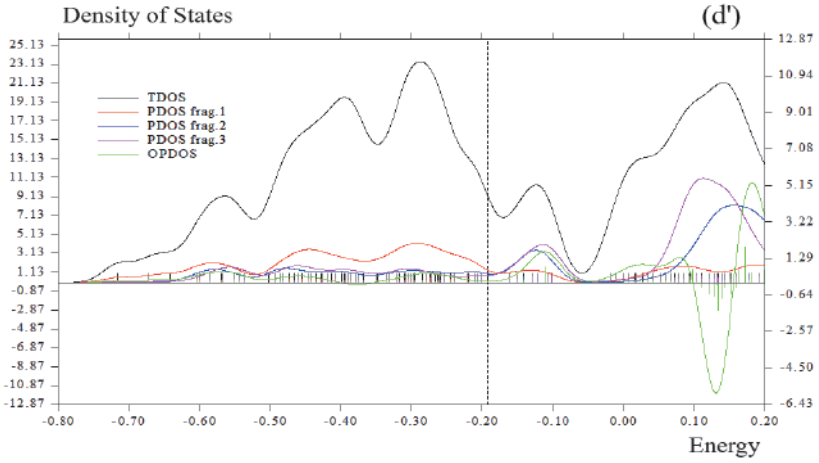
Density of States
(d')
TDOS
PDOS frag.1
PDOS frag.2
PDOS frag.3
OPDOS
25.13 23.13 21.13 19.13 17.13 15.13 13.13 11.13 9.13 7.13 5.13 3.13 1.13 -0.87 -2.87 -4.87 -6.87 -8.87 -10.87 -12.87
12.87 10.94 9.01 7.08 5.15 3.22 1.29 -0.64 -2.57 -4.50 -6.43
-0.80 -0.70 -0.60 -0.50 -0.40 -0.30 -0.20 -0.10 0.00 0.10 0.20
Energy

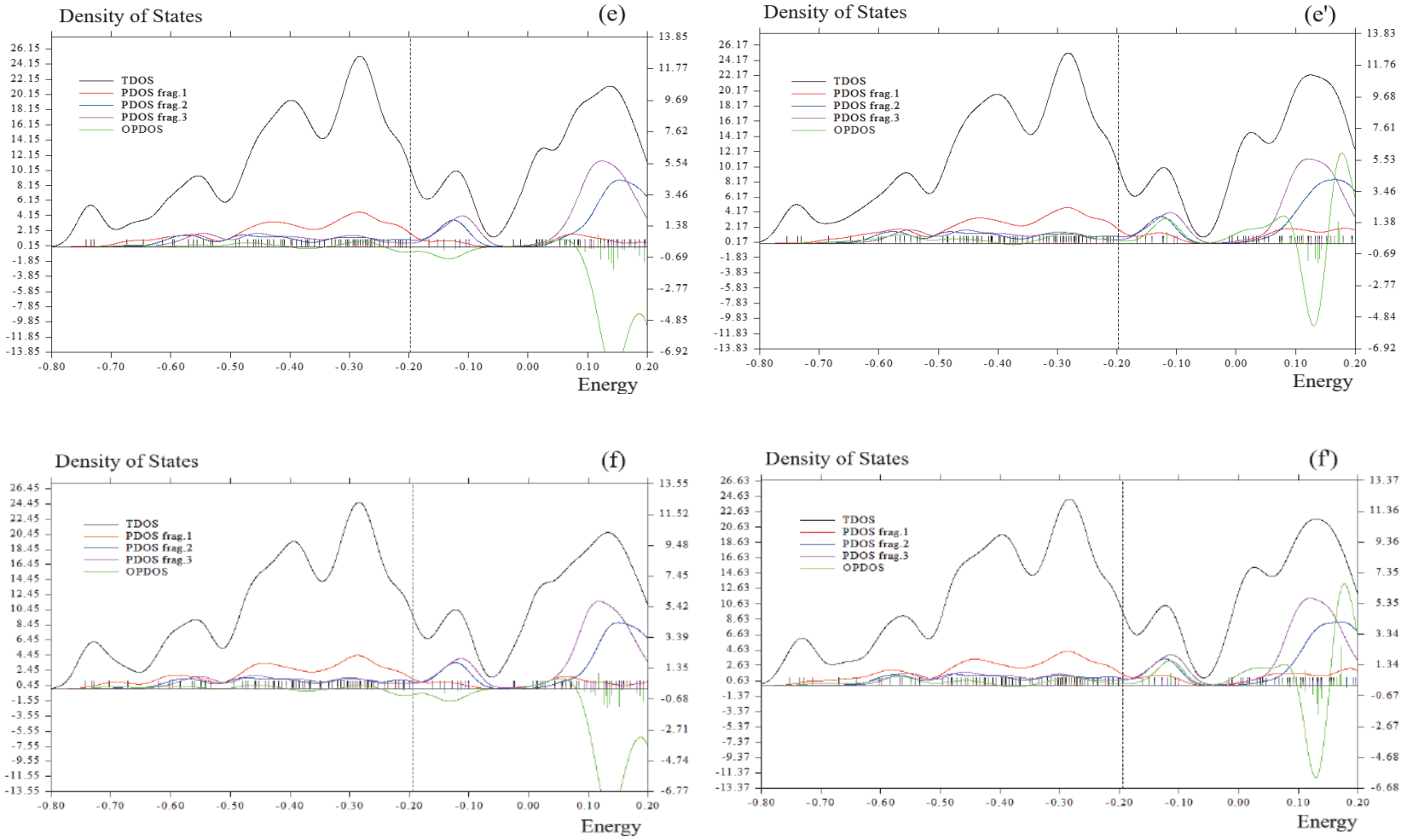

Fig. 3. TDOS/OPDOS graphs of (*a*) LiRb (SnO_2-SiO_2), (*a′*) LiRb(SnO_2-SiO_2)–$2H_2$, (*b*) LiCs(SnO_2-SiO_2), (*b′*) LiCs(SnO_2-SiO_2)–$2H_2$, (*c*) NaRb(SnO_2-SiO_2), (*c′*) NaRb(SnO_2-SiO_2)–$2H_2$, (*d*) NaCs(SnO_2-SiO_2), (*d′*) NaRb(SnO_2-SiO_2)–2H2, (*e*) KRb(SnO_2-SiO_2), (*e′*) KRb(SnO_2-SiO_2)–$2H_2$, (*f*) KCs(SnO_2-SiO_2), (*f′*) KCs(SnO_2-SiO_2)–$2H_2$ nanoclusters

$$D_0(\mathrm{r}) = \frac{3}{10}(6\pi^2)^{2/3}\left[\rho_\alpha\,(\mathrm{r})^{5/3} + \rho_\beta\,(\mathrm{r})^{5/3}\right]. \quad (4)$$

Multiwfn [33, 34] also supports the approximate version of LOL defined by Tsirelson and Stash [35], namely the actual kinetic energy term in LOL is replaced by second-order gradient expansion like ELF which may demonstrate a broad span of bonding samples. This Tsirelson's version of LOL can be activated by setting ELFLOL_type to 1. For special reason, if ELFLOL_type in settings.ini is changed from 0 to 2, another formalism will be used:

$$\mathrm{LOL}(\mathbf{r}) = \frac{1}{1+\left[1/\tau(\mathrm{r})\right]^2}. \quad (5)$$

If the parameter ELFLOL_cut in settings.ini is set to *x*, then LOL will be zero where LOL is less than *x*.

Trapping of hydrogens by LiRb (SnO_2-SiO_2), LiCs(SnO_2-SiO_2), NaRb(SnO_2-SiO_2), NaCs(SnO_2-SiO_2), KRb(SnO_2-SiO_2), KCs(SnO_2-SiO_2) (Fig. 4 *a–f*) nanoclusters towards formation of LiRb(SnO_2-SiO_2)–$2H_2$, LiCs(SnO_2-SiO_2)–$2H_2$, NaRb(SnO_2-SiO_2)–$2H_2$, NaCs(SnO_2-SiO_2)–$2H_2$, KRb(SnO_2-SiO_2)–$2H_2$, KCs(SnO_2-SiO_2)–$2H_2$ might be described by LOL graphs due to achieving their delocalization/localization characterizations of electrons and chemical bonds (Fig. 4 *a′–f′*).

An isosurface map has shown the electron delocalization in LiRb (SnO_2-SiO_2) (Fig. 4 *a*), LiRb(SnO_2-SiO_2)–$2H_2$ (Fig. 4 *a′*), LiCs (SnO_2-SiO_2) (Fig. 4 *b*), LiCs(SnO_2-SiO_2)–$2H_2$ (Fig. 4 *b′*), NaRb (SnO_2-SiO_2) (Fig. 4 *c*), NaRb(SnO_2-SiO_2)–$2H_2$ (Fig. 4 *c′*), NaCs (SnO_2-SiO_2) (Fig. 4 *d*), NaCs(SnO_2-SiO_2)–$2H_2$ (Fig. 4 *d′*), KRb (SnO_2-SiO_2) (Fig. 4 *e*), KRb(SnO_2-SiO_2)–$2H_2$ (Fig. 4 *e′*), KCs (SnO_2-SiO_2) (Fig. 4 *f*), and KCs(SnO_2-SiO_2)–$2H_2$ (Fig. 4 *f′*) through labeling atoms of O10, O12, Si13, O24, O26, Sn28, X31(X = Li, Na or K), Y32 (Y = Rb or Cs) and H33, H34, H35, H36. In fact, the counter map of LOL can confirm that LiRb (SnO_2-SiO_2), LiCs(SnO_2-SiO_2), NaRb(SnO_2-SiO_2), NaCs(SnO_2-SiO_2), KRb(SnO_2-SiO_2), KCs(SnO_2-SiO_2) nanoclusters may increase the efficiency during hydrogen adsorption towards formation of LiRb(SnO_2-SiO_2)–$2H_2$, LiCs(SnO_2-SiO_2)–$2H_2$, NaRb(SnO_2-SiO_2)–$2H_2$, NaCs(SnO_2-SiO_2)–$2H_2$, KRb(SnO_2-SiO_2)–$2H_2$, KCs(SnO_2-SiO_2)–$2H_2$.

Besides, intermolecular orbital overlap integral is important in discussions of intermolecular charge transfer which can calculate HOMO-HOMO and LUMO-LUMO overlap integrals between the H_2 molecules and heteroclusters of LiRb(SnO_2-SiO_2), LiRb(SnO_2-SiO_2)–$2H_2$, LiCs(SnO_2-SiO_2), LiCs(SnO_2-SiO_2)–$2H_2$, NaRb(SnO_2-SiO_2), NaRb(SnO_2-SiO_2)–$2H_2$, NaCs(SnO_2-SiO_2), NaCs(SnO_2-SiO_2)–$2H_2$, KRb(SnO_2-SiO_2), KRb(SnO_2-SiO_2)–$2H_2$, KCs(SnO_2-SiO_2), and KCs(SnO_2-SiO_2)–$2H_2$ nanoclusters.

Table 4. Stability energy (kcal/mol), dipole moment (debye), LUMO (eV), HOMO(eV), and energy gap (ΔE) (eV) for LiRb (SnO_2-SiO_2), LiCs(SnO_2-SiO_2), NaRb(SnO_2-SiO_2), NaCs(SnO_2-SiO_2), KRb(SnO_2-SiO_2), KCs(SnO_2-SiO_2) through hydrogen grabbing and formation of LiRb(SnO_2-SiO_2)–$2H_2$, LiCs(SnO_2-SiO_2)–$2H_2$, NaRb(SnO_2-SiO_2)–$2H_2$, NaCs(SnO_2-SiO_2)–$2H_2$, KRb(SnO_2-SiO_2)–$2H_2$, KCs(SnO_2-SiO_2)–$2H_2$ heteroclusters

Heteroclusters	$E_s\times10^{-3}$ (kcal/mol)	Dipole moment (debye)	E_{HOMO} (eV)	E_{LUMO} (eV)	$\Delta E = E_{LUMO} - E_{HOMO}$, (eV)
LiRb (SnO_2-SiO_2)	-984.9774	5.5566	-5.4115	-4.5381	0.8734
LiRb(SnO_2-SiO_2)–$2H_2$	-986.4044	5.5797	-5.3782	-4.5716	0.8066
LiCs(SnO_2-SiO_2)	-982.3057	6.1309	-5.2868	-4.4110	0.8758
LiCs(SnO_2-SiO_2)–$2H_2$	-983.7106	6.1503	-5.2956	-4.4034	0.8922
NaRb(SnO_2-SiO_2)	-980.3921	5.5542	-5.3875	-4.5210	0.8665
NaRb(SnO_2-SiO_2)–$2H_2$	-981.8157	5.6774	-5.3833	-4.5268	0.8564
NaCs(SnO_2-SiO_2)	-977.7186	6.3330	-5.1992	-4.4149	0.7843
NaCs(SnO_2-SiO_2)–$2H_2$	-979.1183	6.3024	-5.2207	-4.4144	0.8063
KRb(SnO_2-SiO_2)	-997.8810	5.5425	-5.3745	-4.5160	0.8584
KRb(SnO_2-SiO_2)–$2H_2$	-999.2918	5.5675	-5.3844	-4.5357	0.8486
KCs(SnO_2-SiO_2)	-995.2091	6.0936	-5.2494	-4.3767	0.8727
KCs(SnO_2-SiO_2)–$2H_2$	-996.5960	6.0707	-5.2811	-4.3933	0.8879

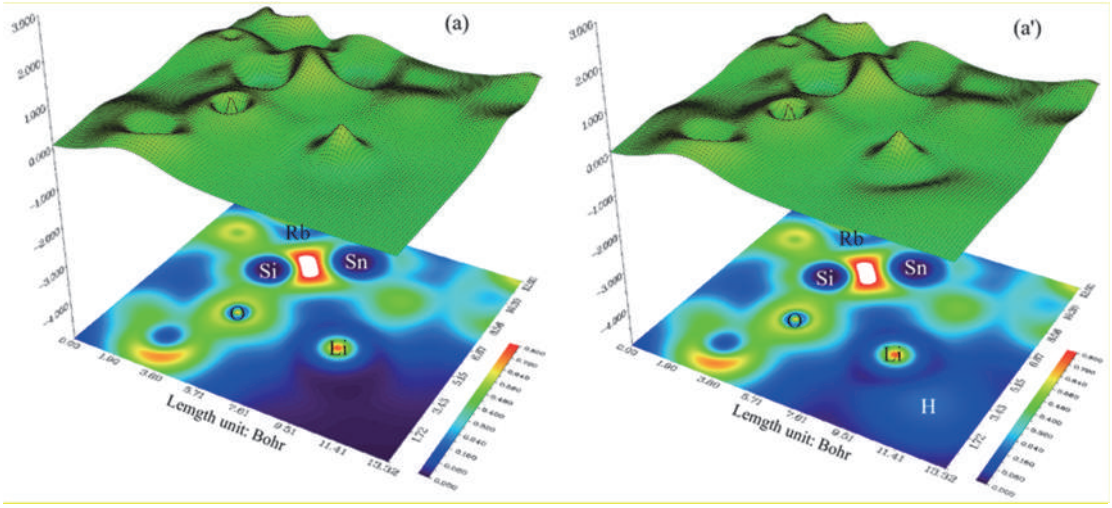
(a)
Rb
Si
Sn
O
Li
Lemgth unit: Bohr
(a')
Rb
Si
Sn
O
Li
H
Lemgth unit: Bohr

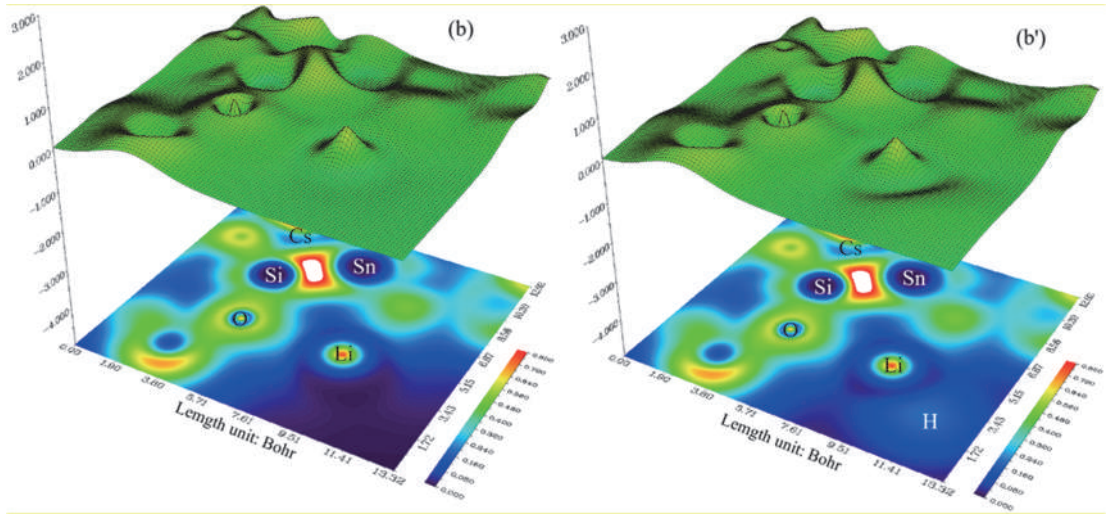
(b)
Cs
Si
Sn
O
Li
Lemgth unit: Bohr
(b')
Cs
Si
Sn
O
Li
H
Lemgth unit: Bohr

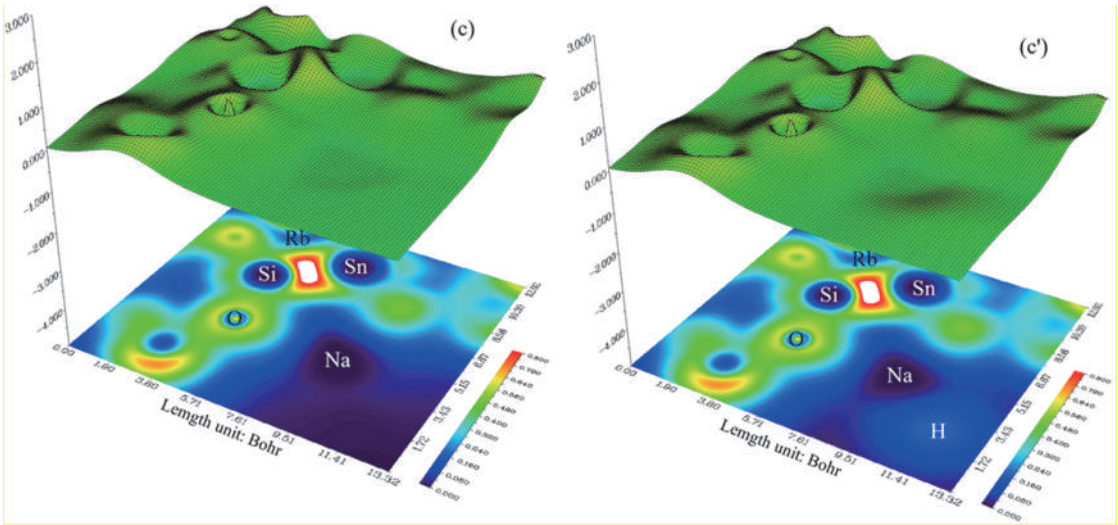
(c)
Rb
Si
Sn
O
Na
Lemgth unit: Bohr
(c')
Rb
Si
Sn
O
Na
H
Lemgth unit: Bohr

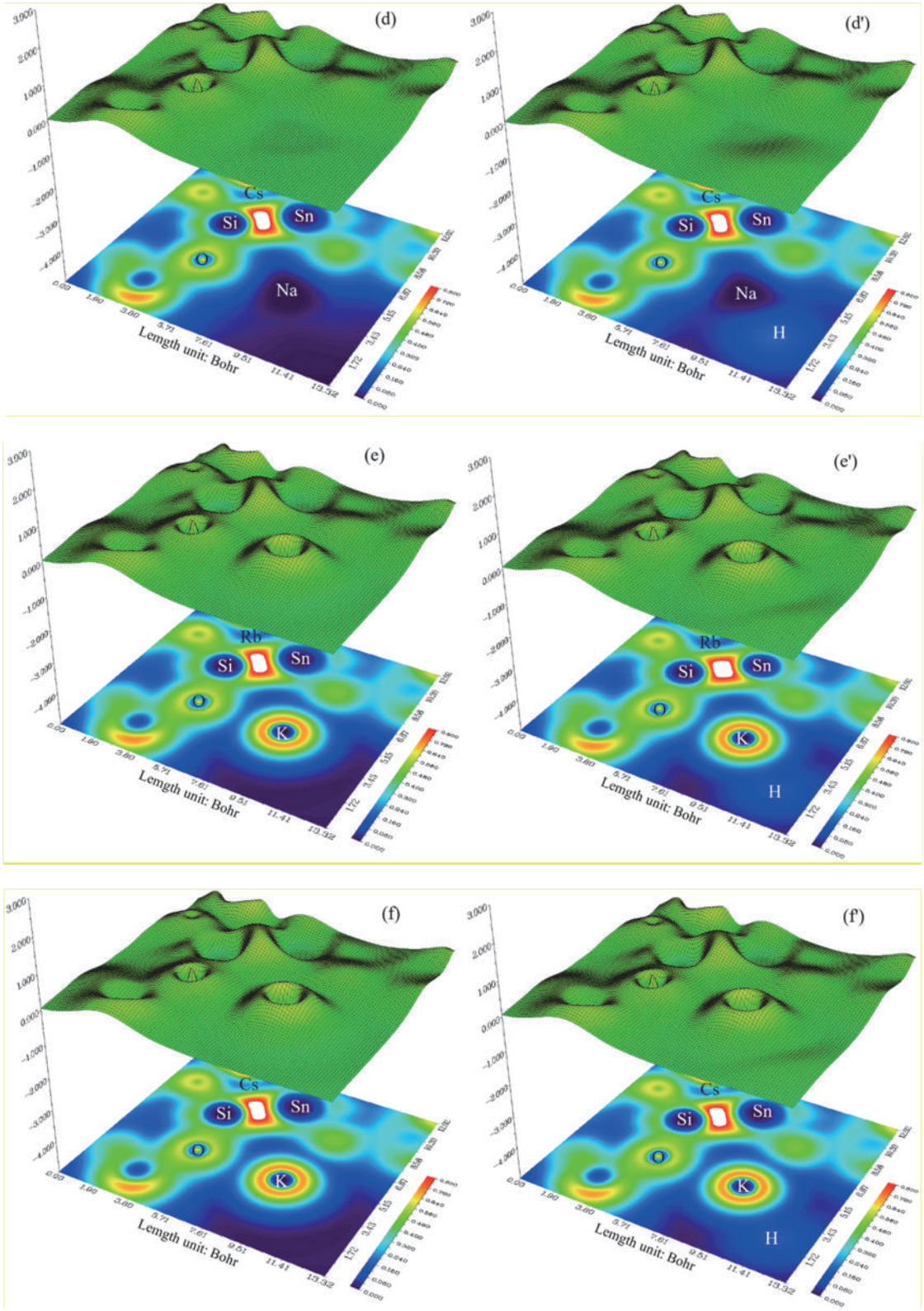

Fig. 4. The counter map of LOL graphs for (*a*) LiRb (SnO_2-SiO_2), (*a′*) LiRb(SnO_2-SiO_2)–$2H_2$, (*b*) LiCs(SnO_2-SiO_2), (*b′*) LiCs(SnO_2-SiO_2)–$2H_2$, (*c*) NaRb(SnO_2-SiO_2), (*c′*) NaRb(SnO_2-SiO_2)–$2H_2$, (*d*) NaCs(SnO_2-SiO_2), (*d′*) NaRb(SnO_2-SiO_2)–2H2, (*e*) KRb(SnO_2-SiO_2), (*e′*) KRb(SnO_2-SiO_2)–$2H_2$, (*f*) KCs(SnO_2-SiO_2), (*f′*) KCs(SnO_2-SiO_2)–$2H_2$ nanoclusters

The applied wavefunction level is CAM–B3LYP–D3/6–311+G (d, p) that corresponds to HOMO and LUMO (Table 4). The layered germanium-silicon oxide improved by alkali metal lithium doping have indicated the structural stability of lithium-, sodium- or potassium-ion batteries through the reported stability energy in Table 4. A small portion of Rb or Cs entered the Sn–Si layer to replace the Li, Na or K sites might improve the structural stability of the electrode material at high multiplicity, thereby improving the capacity retention rate.

In summary, the addition of Rb or Cs ions into electrolyte greatly improves the cycling performance of the hard carbon anode in lithium-, sodium-, or potassium-ion batteries. This improvement is attributed to the participation of the Rb or Cs ions to form a highly conductive, which results in a lower cell reaction resistance. Therefore, the battery cells with Rb or Cs ions as the additive have not only higher specific capacity and smaller polarization, but also more stable.

CONCLUSIONS

H-capture by the nanoclusters of LiRb (SnO_2-SiO_2), LiCs(SnO_2-SiO_2), NaRb(SnO_2-SiO_2), NaCs(SnO_2-SiO_2), KRb(SnO_2-SiO_2), KCs(SnO_2-SiO_2) was investigated by first-principles computations of DFT method. The changes of charge density defined a notable charge transfer in LiRb (SnO_2-SiO_2), LiCs(SnO_2-SiO_2), NaRb(SnO_2-SiO_2), NaCs(SnO_2-SiO_2), KRb(SnO_2-SiO_2), KCs(SnO_2-SiO_2). The fluctuation in charge density values describes that the electronic densities were in the boundary of adsorbate/adsorbent atoms during the adsorption status. Besides, thermodynamic parameters describing H-grabbing by alkali metals-based nanoclusters of LiRb (SnO_2-SiO_2), LiCs(SnO_2-SiO_2), NaRb(SnO_2-SiO_2), NaCs(SnO_2-SiO_2), KRb(SnO_2-SiO_2), KCs(SnO_2-SiO_2) have been studied consisting of internal process of the adsorbent–adsorbate system. The electronegativity, local dipole, and charge transfer are proposed to reveal the doping sites. Li, Na, K bond chemistry further deepens the understanding to exhibit the best charge transfer among single-doped and co-doped atoms, respectively. The excellent charge transfer achieved by Rb, Cs-doping SnO_2-SiO_2 is further validated by Li, Na, K nucleation overpotential measurement.

ACKNOWLEDGEMENTS

In successfully completing this paper and its research, the author is grateful to Kastamonu University.

Моделювання захоплення водню матеріалами на основі SnO_2–SiO_2, легованими лужним металом

Фатеме Моллаамін

Кафедра біомедичної інженерії, факультет інженерії та архітектури, Університет Кастамону Кастамону, Туреччина, fmollaamin@kastamonu.edu.tr

Масштабне дослідження H-захоплення LiRb (SnO_2-SiO_2), LiCs(SnO_2-SiO_2), NaRb(SnO_2-SiO_2), NaCs(SnO_2-SiO_2), KRb(SnO_2-SiO_2), KCs(SnO_2-SiO_2), було проведено в тому числі з використанням DFT обчислень на CAM–B3LYP–D3/6–311+G (d,p) рівні теорії. Гіпотезу явища адсорбції водню було з'ясовано за розподілами густини CDD, TDOS/OPDOS, LOL для нанокластерів LiRb(SnO_2-SiO_2)–$2H_2$, LiCs(SnO_2-SiO_2)–$2H_2$, NaRb(SnO_2-SiO_2)–$2H_2$, NaCs(SnO_2-SiO_2)–$2H_2$, KRb(SnO_2-SiO_2)–$2H_2$, KCs(SnO_2-SiO_2)–$2H_2$. Коливання величини густини заряду показує, що електронна густина була в основному розміщена на краю атомів адсорбат/адсорбент під час стану адсорбції. Щодо оптимізованої енергії, гетерокластери KRb(SnO_2-SiO_2), KRb(SnO_2-SiO_2)–$2H_2$, KCs(SnO_2-SiO_2) і KCs(SnO_2-SiO_2)–$2H_2$ показали більшу стабільність, ніж LiRb(SnO_2-SiO_2), LiRb(SnO_2-SiO_2)–$2H_2$, гетерокластери LiCs(SnO_2-SiO_2), LiCs(SnO_2-SiO_2)–$2H_2$, NaRb(SnO_2-SiO_2), NaRb(SnO_2-SiO_2)–$2H_2$, NaCs(SnO_2-SiO_2), NaCs(SnO_2-SiO_2)–$2H_2$. У цьому дослідженні водневі джерела енергії на функціоналізованих металами двовимірних матеріалах були показані як перспективні альтернативи для систем чистої енергії. Зокрема, ми продемонстрували тут, що (SnO_2-SiO_2) слабко адсорбує H_2. У той же час декорування Li/Na/K значно посилює взаємодію H_2, пристосовуючись до молекул H_2 шляхом сильнішої фізичної абсорбції.

***Ключові слова**: накопичення енергії, лужно-метал-іонний аккумулятор, густина станів, розподіл заряду, моделювання матеріалів, адсорбція водню*

REFERENCES

1. Yang H., Wu N. Ionic Conductivity and Ion Transport Mechanisms of Solid-State Lithium-Ion Battery Electrolytes: A Review. *Energy Sci. Eng.* 2022. **10**(5)*:* 1643.
2. Walvekar H., Beltran H., Sripad S., Pecht M. Implications of the Electric Vehicle Manufacturers' Decision to Mass Adopt Lithium-Iron Phosphate Batteries. *IEEE Access.* 2022. **10**: 63834.
3. Choi D., Shamim N., Crawford A., Huang Q., Vartanian C.K., Viswanathan V.V., Paiss M.D., Alam M.J.E., Reed D.M., Sprenkle V.L. Li-Ion Battery Technology for Grid Application. *J. Power Sources.* 2021. **511**: 230419.
4. Ahmad T., Zhang D. A Critical Review of Comparative Global Historical Energy Consumption and Future Demand: The Story Told so Far. *Energy Rep.* 2020. **6**: 1973.
5. Mlilo N., Brown J., Ahfock T. Impact of Intermittent Renewable Energy Generation Penetration on the Power System Networks–A Review. *Technol. Econ. Smart Grids Sustainable Energy.* 2021. **6**(1): 1.
6. Rautela R., Yadav B.R., Kumar S. A Review on Technologies for Recovery of Metals from Waste Lithium-Ion Batteries. *J. Power Sources.* 2023. **580**: 233428.
7. Tan A.K.X., Paul S. Beyond Lithium: Future Battery Technologies for Sustainable Energy Storage. *Energies.* 2024. **17**(22): 5768.
8. Singh A.N., Islam M., Meena A., Faizan M., Han D., Bathula C., Hajibabaei A., Anand R., Nam K.W. Unleashing the Potential of Sodium-Ion Batteries: Current State and Future Directions for Sustainable Energy Storage. *Adv. Funct. Mater.* 2023. **33**(46): 2304617.
9. Gu Z.Y., Guo J.Z., Cao J.M., Wang X.T., Zhao X.X., Zheng X.Y., Li W.H., Sun Z.H., Liang H.J., Wu X.L. An Advanced High-Entropy Fluorophosphate Cathode for Sodium-Ion Batteries with Increased Working Voltage and Energy Density. *Adv. Mater.* 2022. **34**(14): 2110108.
10. Jin Y., Le P.M.L., Gao P., Xu Y., Xiao B., Engelhard M.H., Cao X., Vo T.D., Hu J., Zhong L., Matthews B.E., Yi R., Wang Ch., Li X., Liu J., Zhang Ji-G. Low-Solvation Electrolytes for High-Voltage Sodium-Ion Batteries. *Nat. Energy.* 2022. **7**: 718.
11. Zhang X., Xiong T., He B., Feng S., Wang X., Wei L., Mai L. Recent Advances and Perspectives in Aqueous Potassium-Ion Batteries. *Energy Environ. Sci.* 2022. **15**(9): 3750.
12. Ge J., Fan L., Rao A.M., Zhou J., Lu B. Surface-Substituted Prussian Blue Analogue Cathode for Sustainable Potassium-Ion Batteries. *Nat. Sustain.* 2022. **5**: 225.
13. Ji B., Yao W., Zheng Y., Kidkhunthod P., Zhou X., Tunmee S., Sattayaporn S., Cheng H.M., He H., Tang Y. A Fluoroxalate Cathode Material for Potassium-Ion Batteries with Ultra-Long Cyclability. *Nat. Commun.* 2020. **11**: 1225.
14. Nazeer W., Farooq A., Younas M., Munir M., Kang S.M. On Molecular Descriptors of Carbon Nanocones. *Biomolecules.* 2018. **8**(3): 92.
15. Zhao J., Li Z., Cole M.T., Wang A., Guo X., Liu X., Lyu W., Teng H., Qv Y., Liu G. et al. Nanocone-Shaped Carbon Nanotubes Field-Emitter Array Fabricated by Laser Ablation. *Nanomaterials.* 2021. **11**(12): 3244.
16. Rong Y., Cao Y., Guo N., Li Y., Jia W., Jia D. A simple method to synthesize V_2O_5 nanostructures with controllable morphology for high performance Li-ion batteries. *Electrochim. Acta*. 2016. **222**: 1691.
17. Yodsin N., Sakagami H., Udagawa T., Ishimoto T., Jungsuttiwong S., Tachikawa M. Metal-doped carbon nanocones as highly efficient catalysts for hydrogen storage: Nuclear quantum effect on hydrogen spillover mechanism. *Mol. Catal.* 2021. **504**: 111486.
18. Taha H.O., El Mahdy A.M., El Sayed El Shemy F., Hassan M.M. Hydrogen storage in SiC, GeC, and SnC nanocones functionalized with nickel, Density Functional Theory – Study. *Int. J. Quantum Chem*. 2023. **123**(3): e27023.
19. Wei T., Zhou Y., Sun C. *et al.* An intermittent lithium deposition model based on CuMn-bimetallic MOF derivatives for composite lithium anode with ultrahigh areal capacity and current densities. *Nano Res.* 2024. **17**(4): 2763.
20. Mollaamin F., Monajjemi M. Nanomaterials for Sustainable Energy in Hydrogen-Fuel Cell: Functionalization and Characterization of Carbon Nano-Semiconductors with Silicon, Germanium, Tin or Lead through Density Functional Theory Study. *Russ. J. Phys. Chem. B.* 2024. **18**: 607.
21. Mollaamin F., Shahriari S., Monajjemi M. Influence of Transition Metals for Emergence of Energy Storage in Fuel Cells through Hydrogen Adsorption on the MgAl Surface. *Russ. J. Phys. Chem. B.* 2024. **18**: 398.
22. Mollaamin F. Competitive Intracellular Hydrogen-nanocarrier Among Aluminum, Carbon, or Silicon Implantation: a Novel Technology of Eco-Friendly Energy Storage using Research Density Functional Theory. *Russ. J. Phys. Chem. B*. 2024. **18**: 805.
23. Che H., Liu J., Wang H., Wang X., Zhang Sh.S., Liao X.-Zh., Ma Zi-F. Rubidium and cesium ions as electrolyte additive for improving performance of hard carbon anode in sodium-ion battery. *Electrochem. Commun*. 2017. **83**: 20.

24. Henkelman G., Arnaldsson A., Jónsson H. A fast and robust algorithm for Bader decomposition of charge density. *Comput. Mater. Sci.* 2006. **36**(3): 354.
25. Mollaamin F., Monajjemi M. Adsorption ability of Ga_5N_{10} nanomaterial for removing metal ions contamination from drinking water by DFT. *Int. J. Quantum Chem*. 2024. **124**(2): e27348.
26. Mollaamin F., Monajjemi M. Molecular modelling framework of metal-organic clusters for conserving surfaces: Langmuir sorption through the TD-DFT/ONIOM approach. *Mol. Simul*. 2023. **49**(4): 365.
27. Vosko S.H., Wilk L., Nusair M. Accurate spin-dependent electron liquid correlation energies for local spin density calculations: a critical analysis. *Can. J. Phys*. 1980. **58**(8): 1200.
28. Frisch M.J., Trucks G.W., Schlegel H.B., Scuseria G.E., Robb M.A., Frisch M.J., Trucks G.W., Schlegel H.B., Scuseria G.E., Robb M.A., Cheeseman J.R., Scalmani G., Barone V., Petersson G.A., Nakatsuji H., Li X., Caricato M., Marenich A.V., Bloino J., Janesko B.G., Gomperts R., Mennucci B., Hratchian H.P., Ortiz J.V., Izmaylov A.F., Sonnenberg J.L., Williams-Young D., Ding F., Lipparini F., Egidi F., Goings J., Peng B., Petrone A., Henderson T., Ranasinghe D., Zakrzewski V.G., Gao J., Rega N., Zheng G., Liang W., Hada M., Ehara M., Toyota K., Fukuda R., Hasegawa J., Ishida M., Nakajima T., Honda Y., Kitao O., Nakai H., Vreven T., Throssell K., Montgomery Jr. J.A., Peralta J.E., Ogliaro F., Bearpark M.J., Heyd J.J., Brothers E.N., Kudin K.N., Staroverov V.N., Keith T.A., Kobayashi R., Normand J., Raghavachari K., Rendell A.P., Burant J.C., Iyengar S.S., Tomasi J., Cossi M., Millam J.M., Klene M., Adamo C., Cammi R., Ochterski J.W., Martin R.L., Morokuma K., Farkas O., Foresman J.B., Fox D.J. Gaussian 16, Revision C.01, Gaussian, Inc., Wallingford CT, 2016.
29. GaussView, Version 6.06.16, Dennington, Roy; Keith, Todd A.; Millam, John M. Semichem Inc., Shawnee Mission, KS, 2016.
30. Xu Z., Qin Ch., Yu Y., Jiang G., Zhao L. First-principles study of adsorption, dissociation, and diffusion of hydrogen on α-U (110) surface. *AIP Adv*. 2024. **14**: 055114.
31. Becke A.D., Edgecombe K.E. A simple measure of electron localization in atomic and molecular systems. *J. Chem. Phys.* 1990. **9**: 5397.
32. Schmider H.L., Becke A.D. Chemical content of kinetic energy density. *J. Mol. Struct. THEOCHEM*. 2000. **27**(1–3): 51.
33. Lu T., Chen F. Multiwfn: A multifunctional wavefunction analyzer. *J. Comput. Chem*. 2012. **33**(5): 580.
34. Lu T. A comprehensive electron wavefunction analysis toolbox for chemists, Multiwfn. *J. Chem. Phys.* 2024. **161**: 082503.
35. Tsirelson V., Stash A. Analyzing experimental electron density with the localized-orbital locator. *Acta Cryst. B.* 2002. **58**(5): 780.

Received 07.03.2025, accepted 04.09.2025